

Graphene Oxide/Polyaniline/Manganese Oxide Ternary Nanocomposites, Facile Synthesis, Characterization, and Application for Indigo Carmine Removal

Ali H. Gemeay¹ · Rehab G. Elsharkawy¹ · Eman F. Aboelfetoh¹

Published online: 9 March 2017
© Springer Science+Business Media New York 2017

Abstract Graphene oxide/polyaniline/manganese oxide ternary nanocomposites (GO/PANI/Mn₂O₃) have been successfully synthesized in one-pot method by in situ chemical oxidative polymerization of aniline in acidic medium using MnO₂ as an oxidant. The obtained nanocomposites have been characterized by transmission electron microscope, Fourier transform infrared, X-ray powder diffraction, and thermogravimetric analysis. The adsorption isotherms of indigo carmine (IC) onto; PANI, GO/PANI, PANI/MnO₂, and GO/PANI/Mn₂O₃ have been evaluated under different adsorption conditions. The adsorption isotherm models of Langmuir, Freundlich, and Temkin were applied and the fit linear was obtained with Langmuir model. It was found that adsorption capacities followed the order: GO/PANI > GO/PANI/Mn₂O₃ > PANI > PANI/MnO₂ with the values of 88.73, 76.40, 60.45 and 22.52 mg/g. Moreover, the kinetics of the adsorption process was investigated and fit linear was obtained with pseudo-second-order model. The adsorption process was exothermic and spontaneous as revealed from the thermodynamic studies.

Keywords Graphene oxide · Polyaniline · Manganese dioxide · Nanocomposites · Adsorption · Indigo carmine

Introduction

Graphene oxide (GO) is one of the most important graphene-based materials. Graphene is made of a single layer

of carbon atoms which are closely packed into honeycomb two-dimensional lattice [1, 2]. The interest in graphene originated from its unique physicochemical properties, notably the exceptionally high surface area, electron and thermal mobility, and mechanical strength. The large surface area with a theoretical value of 2630 m²/g, oxygen-containing surface functionalities such as hydroxyl, carboxylic, carbonyl, and epoxide groups, and high water dispersibility makes GO a material of great interest in adsorption-based technologies as well as in the other fields [3–6]. GO is produced at low cost by chemical oxidation of graphite to graphite oxide and subsequent exfoliation by ultra-sonication [7]. The most common approaches to produce GO from graphite was first developed by Hummer's method which involves using KMnO₄ as an oxidizing agent in concentrated sulfuric acid [8]. The electrostatic interactions of the graphene and GO with an adsorbate make them the materials of choice for adsorption of charged species [5]. Moreover, the presence of oxygen functionalities makes GO as hydrophilic material that can form stable suspensions in aqueous media. This hydrophilic nature when combined with its highest surface area and functional groups density, allowed for a wide variety of chemical functionalization to be performed on GO sheets [6]. In the environmental field, graphene and graphene-based materials have been used to develop novel sorbent or photocatalytic materials for environmental decontamination as building blocks for the next generation of water treatment membranes and as electrode materials for contaminant monitoring or removal [5, 9–11].

Among all conducting polymers, polyaniline (PANI) has attracted much scientific interest owing to its low cost, good electrochemical activity, high thermal stability, and environmentally friendly properties [12, 13]. Typically, PANI has been synthesized by oxidative polymerization

✉ Ali H. Gemeay
agemeay@science.tanta.edu.eg

¹ Department of Chemistry, Faculty of Science, Tanta University, Tanta, Egypt

of aniline in acidic medium using various oxidants such as; $S_2O_8^{2-}$, Fe^{3+} , MnO_4^- , IO_3^- , and $Cr_2O_7^{2-}$ salts, as well as benzoyl peroxide and metal/enzyme, catalyzed H_2O_2 [14, 15]. It is well known that the preparation of r-GO/PANI GO/PANI nanocomposites included: (i) mixing of preformed PANI with r-GO or GO and (ii) in situ chemical polymerization of the aniline monomer solution in the presence of r-GO or GO sheets [16, 17]. Since GO has long been recognized as having strong oxidizing properties, it has been served as an oxidizing agent for oxidative polymerization of aniline [18]. Both of GO and PANI have conjugated π -electrons system, thus, it is interesting to prepare GO/PANI composites from both the fundamental and application points of view.

Manganese oxide is well known as a solid oxidizing agent for a variety of electron donating substances in acidic media due to the presence of manganese ions with different oxidation states. Therefore, it has been reported that MnO_2 could be initiated the polymerization of aniline [19–21]. The reaction involves an electron transfer between the tetravalent Mn^{4+} ion of MnO_2 and the lone pair of electrons of anilinium cation which leads to the formation of aniline radical cation. Thus, this radical cation was considered as the rate-determining step during the polymerization process. The propagation of the polyaniline chain resulted from the radical cation of the oligomer couples with an aniline radical. Besides this, the specifically adsorbed anions on the oxide surface in the acidic polymerization bath could be worked as the charge compensator for the positively charged PANI chain and the formation of PANI/ MnO_2 composites [19, 22].

Polyaniline itself has extensive use in the removal of toxic water pollutants such as heavy metals and organic dyes [23–25]. The hybrid materials based on the combination of GO and PANI provided a synergistic effect of improving the PANI conductivity and also mitigating the GO aggregation [26]. These hybrid composites have widely been used for various applications [17–21]. In particular, GO nanosheets when compounded with conducting polymers has enhanced not only the electrical conductivity but also the mechanical strength, adsorptive capacity, catalytic activity, and energy storage of resulting composites [27]. These exciting characteristics enable graphene-based conducting polymer composites to be prime candidates for various applications. To date, extensive efforts and many approaches have been developed to prepare graphene-based composites, especially, GO-PANI or graphene-PANI composite powders, which have exhibited various functional properties [22–24]. Most of the prepared composite products have both pros and cons. Therefore, the effort for new methodologies to prepare hybrids with the aim of further enhancing those properties needs to be developed.

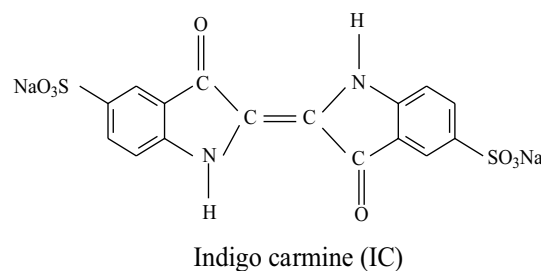
Indigo carmine (IC) is one of the oldest dye used mostly for cotton clothes dyeing (blue jeans) [28]. It is considered as a highly toxic dye that can cause skin and eye irritations [29]. It is also known to cause mild to severe hypertension cardiovascular and respiratory effects in patients [30]. Therefore, the residue of indigo dye-containing wastewater, especially textile effluent, must be treated before being discharged into the environment [9, 31, 32]. Several processes have been suggested for removal of Indigo Carmine. The decolorization of the indigo carmine dye was investigated by various advanced oxidation technologies, such as Fenton reagent [33], electrochemical oxidation [34] and photoassisted oxidation [35].

The present work deals with a one-pot process for the facile synthesis of GO/PANI/ Mn_2O_3 composites by in situ polymerization of aniline monomer using MnO_2 as an initiator in acidic medium. The synergistic effects of polyaniline, MnO_2 , and the high specific surface area of GO are expected to achieve a high performance as a new adsorbent for organic dyes pollutants such as indigo carmine.

Experimental

Materials

Powdered flake graphite (12,500, 500 mesh) was purchased from LOBA Chemie (India). H_2O_2 (30% w/v, Merck, Germany), HCl (36.5%), H_2SO_4 (98%), $KMnO_4$, and aniline were supplied from El-Nasr Chemicals Co. (ADWIC, Egypt). Aniline was distilled under reduced pressure and stored in the dark below 4 °C. β - MnO_2 (99%, Riedel de Haen) of specific surface area of 20 m^2/g was used as received. Indigo carmine (IC) (disodium salt of 3,3-dioxobi-indolin-2,2-ylidene-5,5-disulfonate), C. I. 73,015, Molecular weight equals 466.35, was obtained from Sigma-Aldrich. The standard solutions and dilution were made using doubly distilled water following the standard procedures.



Synthesis of Graphene Oxide

Graphene oxide was synthesized via the modified Hummer's method [36, 37]. Typically, graphite flakes (3 g) and NaNO_3 (3 g) were added in 150 mL of concentrated H_2SO_4 in 250 mL flask and stirred in ice bath for 30 min. After that KMnO_4 (9.0 g) was added slowly in small portions to keep the reaction temperature below 20°C in order to prevent the overheating and explosion. The reaction was warmed to 35°C and stirred for 3 h until it became thickened [38]. The resulting mixture was poured into 400 mL of ice under vigorous stirring. Thirty milliliters of H_2O_2 solution (30% v/v) were added slowly to the reaction mixture until gas evolution was stopped. The resulting mixture was centrifuged at 4000 rpm, and the supernatant was decanted away. The yellow–brown GO residue was then washed repeatedly with 5% HCl solution until the washing solvent gave a negative test for the sulfate and chloride ions. The residue obtained after repeated washing was further washed with small amount of distilled water and dried under vacuum for 24 h to get the yellow–brown powder of GO.

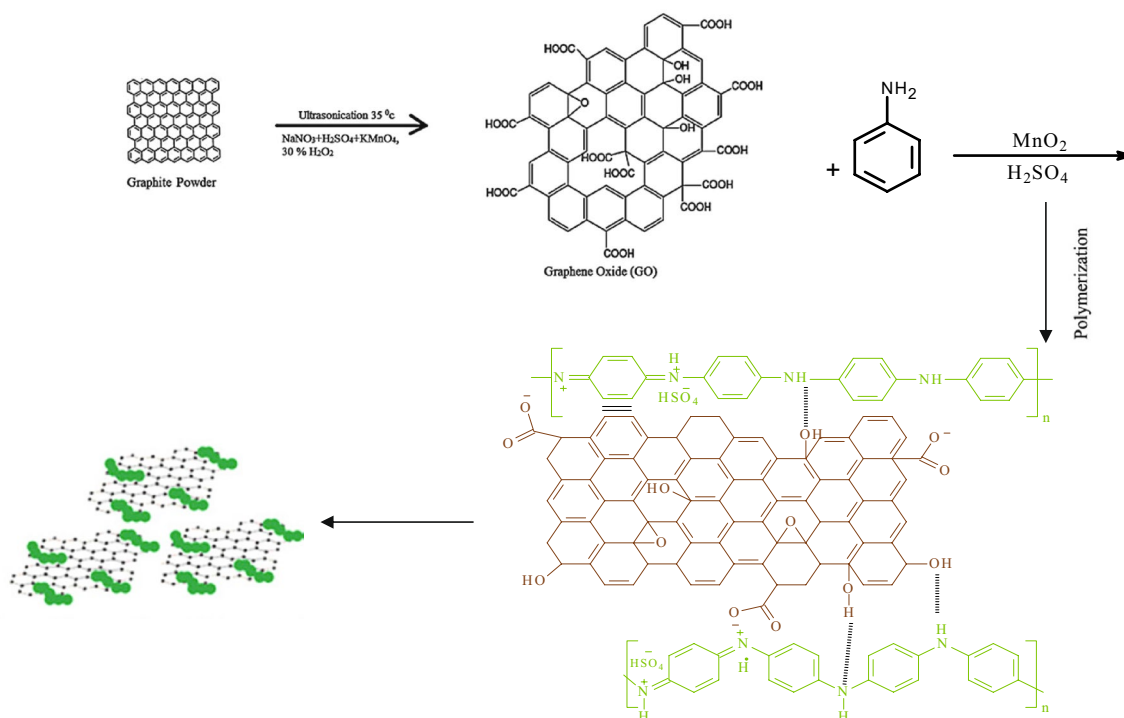
Preparation of GO/PANI/ Mn_2O_3 Composites

GO/PANI/ Mn_2O_3 composites were prepared via in situ polymerization of aniline monomer in a suspension containing GO and MnO_2 in H_2SO_4 solution of 1 M

(Scheme 1). In brief, aniline 3 mL was injected into the polymerization vessel containing 100 mL of an aqueous acid solution containing 1.5 g of suspended MnO_2 and 0.5 g of GO at room temperature. The weight ratio of GO to aniline was 3:7 and the molar ratio of $[\text{ANI}]:[\text{MnO}_2]$ was equal to 0.8:1. The polymerization reaction was initiated immediately after injection of aniline and the mixture was stirred for 1 h at room temperature. The dark-green precipitate was collected by filtration, washed with the acid solution until the filtrate solution becomes clear. Then it was washed repeatedly with acetone and distilled water several times and finally was dried at 50°C for 12 h. The same procedure was followed for preparation of PANI/ MnO_2 and PANI using $(\text{NH}_4)_2\text{S}_2\text{O}_8$ as an initiator instead of MnO_2 in absence of GO.

Instrumentation

The surface morphology of samples was examined using transmission electron microscope (TEM), JEOL-TEM “100-SX” and scanning electron microscope (SEM), Jeol-JSM- 6510 TV. The FTIR spectra were recorded on an FTIR-8400S instrument (Shimadzu) using the KBr pellets of the samples. X-ray diffraction (XRD) patterns of the samples were measured on GNRAPD-2000 PRO diffractometer with monochromatic CuK_α radiation ($\lambda=1.54 \text{ \AA}$), a generator voltage 40 kV and current 30 mA at a step



Scheme 1 In situ polymerization of aniline in a suspension containing GO and MnO_2 in H_2SO_4 solution

scan mode. Thermogravimetric analysis (TGA) was done with Perkin Elmer, STA 6000, in the temperature range 25–1000 °C with a heating rate of 10 °C/min under N₂ environment. The samples were ultrasonicated using Cole-Parmer 8851 ultrasonic. The kinetic measurements were monitored spectrophotometrically using a T80+ UV/Vis double beam spectrophotometer (PG Instruments, UK).

Adsorption Measurements

The adsorption experiments of IC were performed in a batch process and conducted in duplicate at 30 ± 0.2 °C in a temperature-controlled shaker. Typical, 5 mg of the composite was firstly dispersed in 10 mL of doubly distilled water and ultrasonicated for 15 min, then 10 mL of the desired initial concentration of IC (37–55 mg/L) was added under agitation at 120 rpm. At predetermined time intervals, the ternary composite was removed from the solution by centrifugation and the residual IC was determined by using UV/Vis spectrophotometer at $\lambda_{\max} = 610$ nm. The amount of IC adsorbed per unit mass of adsorbent (mg/g) at time *t*, (*q_t*) and the removal percent (*R* %) was calculated from the mass balance equations (1 and 2);

$$q_t = (C_0 - C_t) V/m \quad (1)$$

$$R(\%) = (C_0 - C_t) / C_0 \times 100 \quad (2)$$

where *C₀* and *C_t* are the initial and equilibrium concentrations of dye solution (mg/L) at time *t*, respectively. *V* is the volume of solution (L), and *m* is the mass per gram of ternary composites.

Results and Discussion

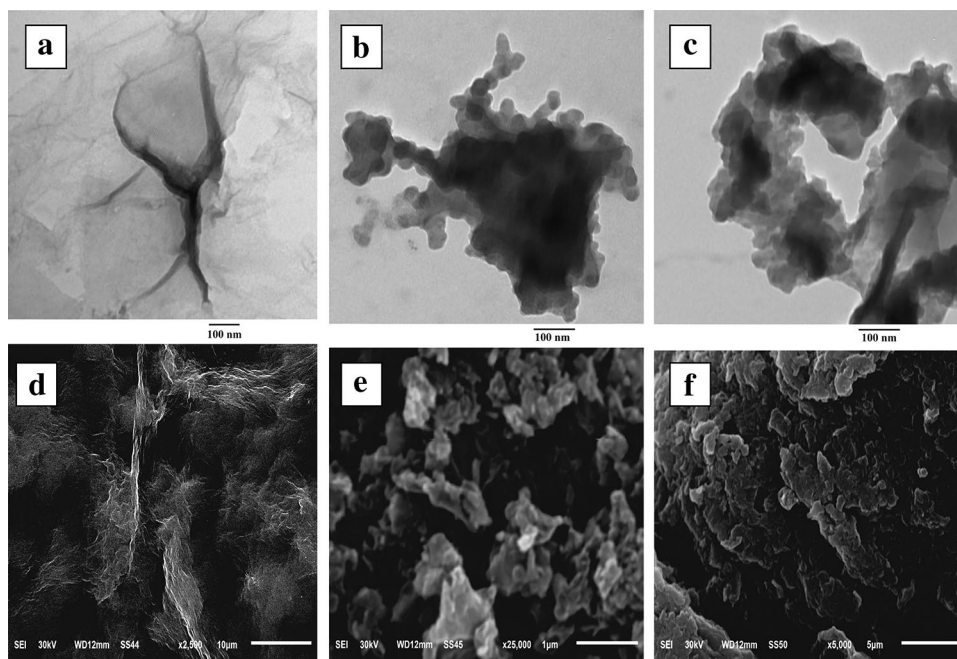
Characterization of Composites

To verify the coexistence of GO, MnO₂, and PANI in the as-prepared composites, several techniques including TEM, SEM, XRD, FT-IR, and TGA have been utilized to identify the hybridized nature of the GO/PANI/Mn₂O₃ ternary composites.

Transmission Electron Microscope (TEM)

To obtain insight into the nanosheet morphology of GO and the hybrid, as well as the layer structures, including the layer exfoliation pattern, transmission electron microscopy (TEM), was used. Exfoliated GO sheets feature transparent wrinkled paper—like the structure of GO implying that a single or few layers of GO have been successfully prepared as depicts in the TEM image (Fig. 1a), while PANI formed a compact layer on top of GO sheets, Fig. 1b. This can be attributed to the disruption of the planar sp² carbon sheets by the introduction of sp³-hybridized carbon upon oxidation, which is consistent with several previous reports [36]. For the GO/PANI nanocomposite, the coating of PANI is clearly visible and distinguishes from the highly crystalline graphitic support, which is attributed to the surrounding of PANI on the GO host. In addition, it could be seen that each flaky layer of the GO is uniformly piled up while layers of the composite have individual directions due to the influence of PANI, indicating that the in situ polymerization affects the structure of GO in an ordered way. A close look

Fig. 1 TEM images of **a** GO, **b** GO/PANI, and **c** GO/PANI/Mn₂O₃ nanocomposites; SEM images of **d** GO, **e** GO/PANI, and **f** GO/PANI/Mn₂O₃



at the TEM images of (Fig. 1c), one would clearly observe the existence of MnO_2 particles, presenting a length less than 100 nm and a diameter of 20 nm.

Scanning Electron Microscope (SEM)

Figure 1d–f shows the SEM images of GO, GO/PANI, and GO/PANI/ Mn_2O_3 composites which exhibit different morphology. As shown in Fig. 1d, the GO sheets composed of a few layers stacked slackly and are creased like silk veil, which may be attributed to strong π - π stacking between GO layers [39]. Moreover, we could notice that the PANI protuberances coat the whole surface of the GO, and those have been much formed at the periphery than the center of the GO. Also, the morphology of the in-situ prepared PANI self-assembled on GO sheets like a broccoli composed numerous of small flower buds, Fig. 1e. While for GO/PANI/ Mn_2O_3 , Fig. 1f, it is noticed that there are no visible big granular particles of PANI on the GO sheets indicative of tiny PANI species growing along GO in GO/PANI/ Mn_2O_3 nanocomposite. Moreover, it is clearly seen that the surface of GO/PANI/ Mn_2O_3 is much rougher than pristine GO. Also, it is difficult to distinguish the individual phases, i.e. GO and PANI in GO/PANI nanocomposite from the SEM micrograph, which is in good consistent with the obtained TEM images and indicated that most of GO sheets are decorated with polyaniline layer. These can be explained by the adsorption and intercalation of PANI on the surface and between GO sheets [18]. The possible combining mode of graphene oxide/PANI composite is proposed including (a) π - π stacking (b) electrostatic interactions, and (c) hydrogen bonding [15], as presented in Scheme 1, while the presence of MnO_2 particles and their surface adsorbed ions could be functioned as dopant ions for PANI chains as has been reported in our previous work [19].

FT-IR Spectra

FTIR spectra measurements are used to qualitatively determine the characteristic functional groups, which could be making the adsorption process possible. The FTIR spectra of GO, PANI, GO/PANI, PANI/ MnO_2 , and GO/PANI/ Mn_2O_3 are shown in Fig. 2, the peaks at 3420 cm^{-1} for all samples are assigned to the -OH group stretching. As can be seen, the spectrum of GO showed the peaks at 1400 and 1100 cm^{-1} are assigned to asymmetric -COOH stretching vibration, and stretching of C-O bond situated at the edges of the GO sheets, respectively [40]. Also, GO displays distinct vibrational modes of epoxide C-O-C (877 cm^{-1}), ethers (C-O) (900 – 1100 cm^{-1}), epoxide C-O-C (1136 cm^{-1}), epoxide and hydroxyl (C-O-C and C-OH) (1247 cm^{-1}), ketone C=O (1280 – 1500 cm^{-1}),

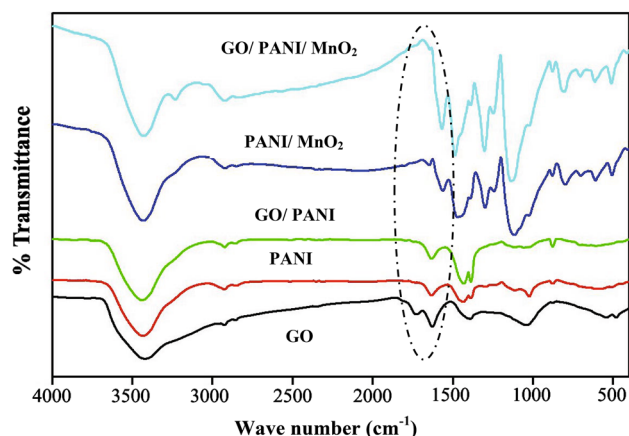


Fig. 2 FTIR spectra of GO, PANI, GO/PANI, PANI/ Mn_2O_3 , and GO/PANI/ Mn_2O_3 nanocomposites

sp^2 -hybridized C=C (1500 – 1600 cm^{-1}), and ketone (C=O) (1620 , 1735 , and 1750 – 1850 cm^{-1}) [41]. The characteristic peak of GO associated with the stretching at 1727 cm^{-1} was also observed at 1630 cm^{-1} is attributed to aromatic C=C bonds. These characteristics indicate the successful grafting of functional groups (i.e. epoxide, hydroxyl, and carboxyl) on the graphite powers to form GO through the oxidation reaction. The existence of PANI can be confirmed by the stretching vibration bands at 1561 cm^{-1} (C=C, quinoid rings), 1492 cm^{-1} (C=C, benzenoid rings), 1287 cm^{-1} (C-N), and 1083 cm^{-1} (C-H) (Fig. 2) [42]. The C=O stretching vibration in GO (1721 cm^{-1}) is disappeared in GO/PANI composite, while the characteristic -NH bending vibration at 1500 – 1600 cm^{-1} is observed [31]. In the composites, all the characteristic peaks of PANI are observed and it confirms the formation of doped PANI in the composites. These results confirmed that the GO sheets were wrapped with PANI.

Moreover, the spectrum of PANI synthesized by MnO_2 as an oxidant in PANI/ MnO_2 and GO/ MnO_2 /PANI nanocomposites are different from the spectra of PANI prepared by $(\text{NH}_4)_2\text{S}_2\text{O}_8$ in some features as shown in Fig. 2. The peak at 528 cm^{-1} can be attributed to Mn-O stretching vibration which confirms the presence of MnO_2 and in good agreement with that reported elsewhere [43]. Furthermore, the FT-IR spectra of the GO/ MnO_2 /PANI composites prepared using at different amounts of MnO_2 are recorded and their characteristics vibration bands are red-shifted as the amount of MnO_2 increased in the polymerization bath, Table 1. This can be attributed to that; (i) the acidity of composite was increased with increasing of MnO_2 due to the adsorption of SO_4^{2-} anions onto MnO_2 surface and worked as charge compensation for PANI chains, (ii) the formation of hydrogen bonding between surface hydroxyl groups of MnO_2 and the amines, charged amines or imine

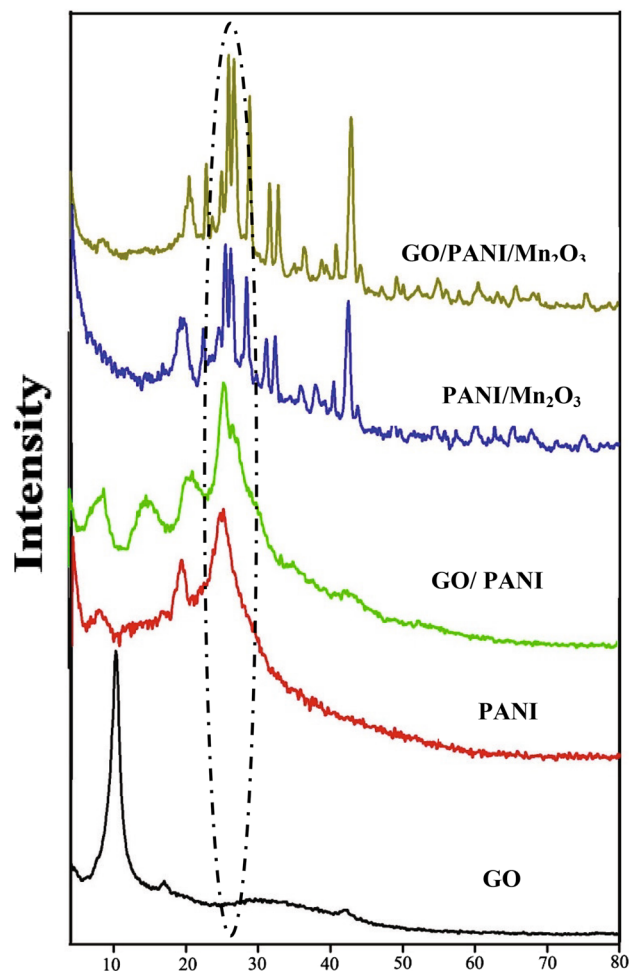
Table 1 Characteristic FT-IR bands (cm^{-1}) of GO/PANI/ Mn_2O_3 composites prepared using: different amount of MnO_2 ; (A) 1.5 g, (B) 2 g and (C) 2.8 g suspended in polymerization bath as an oxidizing agent, 0.64 M of ANI, in the presence of 1.15 M of H_2SO_4 , at 25 °C after 1 h

| Composite | ($-\text{NH}_2^+$)st | $\gamma(-\text{CH}_2)$ st | Quinoid ring | C-Cst | (C— N^+)st | Benzene ring deformation | SO_4^{-2} |
|-----------|------------------------|---------------------------|--------------|-------|----------------------|--------------------------|--------------------|
| A | 3429 | 2923 | 1568 | 1487 | 1247 | 806 | 1136 |
| B | 3422 | 2964 | 1577 | 1494 | 1253 | 819 | 1150 |
| C | 3431 | 2970 | 1570 | 1497 | 1255 | 821 | 1116 |

sites of PANI chains, which has been reported in our previous work [44]. Therefore, the FT-IR spectra verify the coexistence of GO, PANI, and MnO_2 in the as-prepared nanocomposites.

X-ray Diffraction

Typical X-ray diffraction (XRD) patterns of as-synthesized GO, PANI, GO/PANI, PANI/ Mn_2O_3 , and GO/PANI/ Mn_2O_3 composites are shown in Fig. 3. The intensive XRD pattern of GO around $2\theta = 10.72^\circ$ corresponds to the (001) reflection, and the interlayer spacing (0.87 nm) was much larger than that of pristine graphite (0.34 nm). This can be attributed to the insertion of oxygen-containing functional groups on the graphite sheets. As can see the characteristic peak of GO disappears in all other composites, which demonstrates that GO might be reduced to r-GO during the polymerization process as has been reported elsewhere [18]. Also, as shown in Fig. 3, pristine PANI (synthesized using $(\text{NH}_4)_2\text{S}_2\text{O}_8$ as an oxidant) revealed a typical crystalline pattern, which is similar to that of the GO/PANI composite. The diffraction peaks at 2θ equals; 21.17° , 23.70° , 25.43° , and 29.71° represents the emeraldine PANI salt [15, 45]. Moreover, these results showed that PANI has a highly ordered crystal structure, which improves the crystallinity of the composite considerably. The decreases of the peak height of the GO planes in the composite might be caused by the PAN polymer coating of the GO sheets. This can be ascribed to the following reasons; (i) the intercalation of PANI chains between GO sheets, (ii) the grafting of various functional groups (i.e. epoxide, hydroxyl, and carboxyl) and the larger interspacing distance between GO sheets. The comparison of the XRD patterns peaks of GO/PANI/ Mn_2O_3 and GO/PANI composites are shown in Fig. 3. It is revealed that GO/PANI is a more pronounced crystalline phase. This increase in the crystallinity may be attributed to the increase in the PANI % in the resulting composite. The effect of changing the amount of MnO_2 on the degree of crystallinity of the prepared composites has been considered. The interlayer spacing (d) and the free interlayer spacing (Δd) compared with pure PANI/ Mn_2O_3 are included in Table 2. It is notable that increasing the amount of MnO_2 as an oxidant in the polymerization bath led to an increase

**Fig. 3** XRD spectra of GO, PANI, GO/PANI, PANI/ Mn_2O_3 , and GO/PANI/ Mn_2O_3 nanocomposites**Table 2** Interlayer spacing of GO/PANI/ Mn_2O_3 composites prepared using; 1.5 g (A), 2 g (B), and 2.8 g (C) of MnO_2 suspended in polymerization bath as an oxidizing agent, 0.64 M of ANI, in the presence of 1.0 M of H_2SO_4 , at 25 °C after 1 h

| Composite | d Å | Δd Å |
|-------------------------------|--------|--------------|
| PANI/ Mn_2O_3 | 3.0958 | — |
| A | 3.3802 | 0.2844 |
| B | 4.4979 | 1.4021 |
| C | 5.1589 | 2.0631 |

in the % PANI as well as to the increase of the molecular weight of PANI which associated with an increase in the crystallinity. This result is in a good agreement with that reported elsewhere [46, 47].

Thermogravimetric Analysis

Figure 4 depicts the TGA curves of GO, GO/PANI, and GO/PANI/Mn₂O₃ composite. For GO curve, it is clear that there are three obvious weight loss stages. The first step is from room temperature to about 120 °C which can be attributed to the dehydration and evaporation of H₂O molecules from the interlayer of GO. The second one is from 120 to 220 °C, which is due to the burning decomposition of oxygen functional groups on the GO sheets [18, 48]. These oxygen-containing functional groups not only enhance the dispersibility of GO but can also enhance the anchoring of PANI onto GO sheets. The weight loss starting from 208 to 500 °C for GO can be assigned to the combustion of its carbon skeleton as well as the burning of more stable oxygen functionalities [49]. It's been reported that carboxyl groups could probably be removed at this region due to the higher temperature that breaking the double bond between carbon and oxygen of the carboxyl groups. The GO/PANI and GO/PANI/Mn₂O₃ nanocomposites showed similar decomposition curves although the GO/PANI/Mn₂O₃ showed better thermal stability with less weight loss compared with GO/PANI composite. This can be attributed to the presence of Mn₂O₃, which is highly thermal stable [50]. Figure 4 shows that the moisture and dopant anions SO₄²⁻ contents of the two GO/PANI and GO/PANI/Mn₂O₃ composites were around 9.18%, 12.70% (ΔY_1) and 11.96%, 15.28% (ΔY_2), for GO/PANI/Mn₂O₃ and GO/PANI, respectively. To estimate how many aniline repeating units doped with 1 SO₄²⁻ anion in PANI, Eq. (3) is used [51]:

$$\frac{100 - \Delta Y_1 - \Delta Y_2}{\Delta y_2} = \frac{M_1 x X}{M_2 x 1} \quad (3)$$

where ΔY_1 and ΔY_2 are the weight losses of moisture and dopant SO₄²⁻ anions, respectively; M₁ and M₂ are the molecular weights of aniline and dopant SO₄²⁻ anion, respectively; and X is the number of anilines repeating units. Therefore, according to Eq. (3), ΔY_1 , ΔY_2 , M₁, and M₂ are substituted with 9.18, 11.96, 92, and 96, respectively. The value of X at around 6.94 for GO/PANI/Mn₂O₃, while for GO/PANI the X value at around 5.00. This implied that there were roughly six aniline repeat units, on average, doped with SO₄²⁻ anions. The major weight loss (~30%) appears before 600 °C was related to the degradation and decomposition of PANI with different degrees of polymerization. Therefore, TGA suggested that the thermal stability of the composites followed the order: GO/PANI/Mn₂O₃ > GO/PANI > GO. This might be due to the strong interactions between GO and PANI, which impose a restriction on the decomposition of the oxygen groups remaining on the GO surface. These interactions can result in homogeneous heating and the avoidance of heat concentrations [52].

The Interaction Between PANI and GO Sheets

The growth mechanism of GO/PANI nanocomposites can be summarized as follows: (i) Firstly the formation of anilinium cation, (ii) then, ANI⁺ would adsorb well on the GO surfaces and the subsequent in-situ growth of polyaniline chains which would block the re-stacking of the GO sheets [15, 42]. (iii) The possible combining mode of graphene oxide/PANI composite is proposed including (a) π - π stacking (b) electrostatic interactions, and (c) hydrogen bonding, as presented in Scheme 2. The presence of the hydrogen bonds is due to the oxygen and nitrogenous functional groups in the composite. In addition, MnO₂ could be converted into Mn₂O₃ due to its redox reaction during the polymerization of aniline. Moreover, the adsorbed SO₄²⁻ anions onto Mn₂O₃ surface could be working as dopant anions for PANI chains, as had been reported in our previous work [19].

Adsorption Efficiency

As soon as the IC was charged to the GO/PANI or GO/PANI/Mn₂O₃ nanocomposites, a fast drop in the absorbance of the IC was observed within the first minute of contact. The absorbance then continued to decrease gradually with the lapse of time (Fig. 5). Such decrease in absorbance was accompanied with color removal along the time of contact which sometimes extended to 2 h. During this period, the absorbance of IC was declined to ca. 80–85%

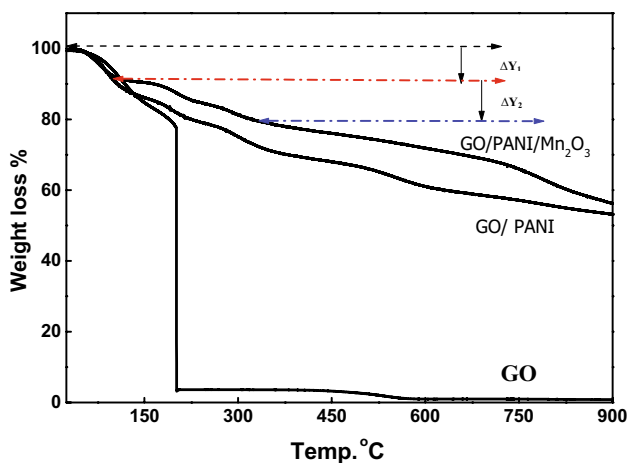


Fig. 4 TGA analysis of GO, GO/PANI, and GO/PANI/Mn₂O₃ nanocomposites

Scheme 2 Illustration of the suggested adsorption mechanism of IC onto GO/PANI composite

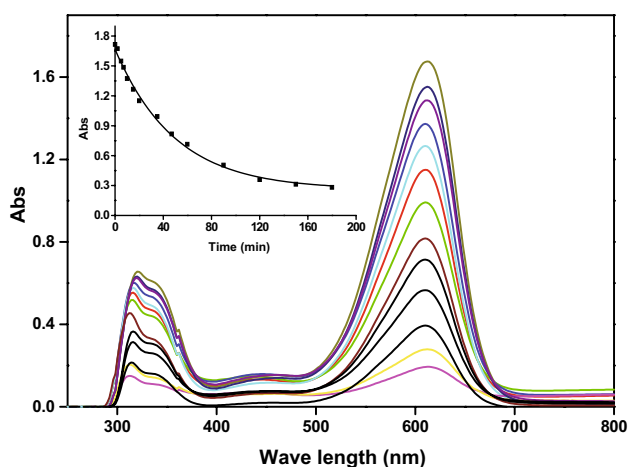
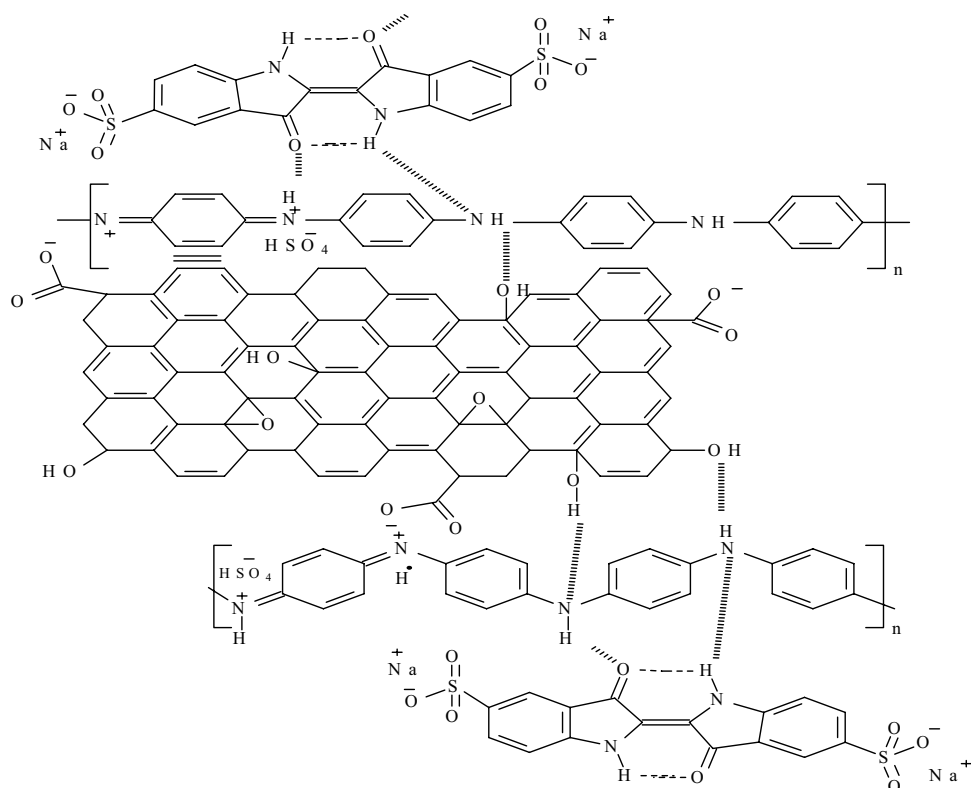


Fig. 5 The decrease in the absorbance of IC during the adsorption progress

of its original value, depending on the reaction conditions applied. The rate of dye removal was a function of several factors. In order to investigate these factors, the kinetics of GO/PANI composites/IC interaction was performed. The UV/Vis absorption spectra of IC solution were recorded in the range 200–800 nm. The concentration of residual IC in solution was calculated using the molar extinction coefficient ($\epsilon = 16,365 \text{ L}\cdot\text{mol}^{-1}\text{cm}^{-1}$) determined experimentally

from Beer–Lambert plot at $\lambda_{\text{max}} = 610 \text{ nm}$. The adsorbed amount (mg/g) of IC at time t , q_t , was calculated from the mass balance Eq. (4).

$$q_t = (C_0 - C_t) V/m \quad (4)$$

where C_0 and C_t are the initial and liquid-phase concentrations of IC (mol/L) at zero and time t , respectively, V is the volume of solution (L), and m is the mass per gram of GO/PANI composites. Adsorption isotherms were established using 0.005 g of GO/PANI composites and the IC dye concentration within the range of 36–55 mg/L. The experiments were carried out at 25, 30, 35, and 40 °C in a temperature-controlled shaking water bath to evaluate the equilibrium constant (K_c) and the corresponding thermodynamic parameters.

A comparison of the q_e values of the tested adsorbents is depicted in Fig. 6, and reveals the following order; GO/PANI > GO/PANI/Mn₂O₃ > PANI > PANI/Mn₂O₃ with the values of; 70.2, 65.7, 60.59, and 19.96 mg/g, respectively. These results indicate that the presence of GO sheets on GO/PANI or GO/PANI/Mn₂O₃ nanocomposites can be the main factor for enhancement the adsorption of IC, suggesting that GO has higher adsorptivity for IC than PANI alone or PANI/Mn₂O₃ nanocomposites. It has been reported that the coexistence of ionic groups and aromatic sp² domains allow GO sheets to participate in wide range of bonding and interactions [38, 53]. Moreover, the formation

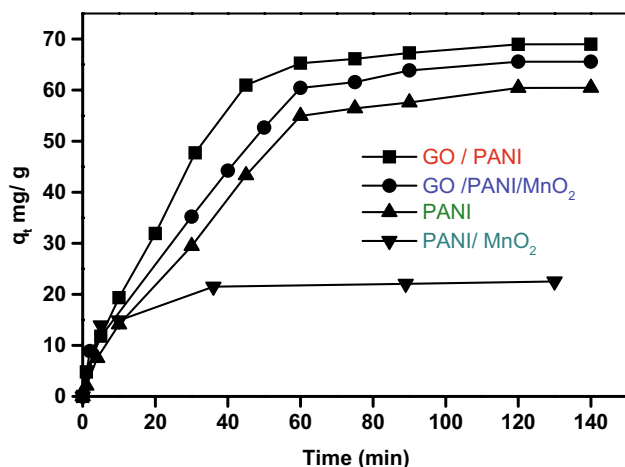


Fig. 6 Pre-equilibrium amount of IC dye adsorbed onto different composites (5 mg) as a function of contact time at 30 °C, $[IC]_0 = 45.61 \text{ mg/L}$

of π - π stacking between IC and aromatic regions of the GO in the PANI/GO composite, the physical adsorption of IC molecules can be promoted. As shown in Fig. 6, the removal of IC in the presence of all adsorbents was found to proceed via two steps. The first is mainly related to the gradual and rapid increase in q_t values with increase in the time of adsorption due to the availability of adsorbent surface active sites as well as the existence of surface pores for IC adsorption. This initial step required about 60 min for attending pre-equilibrium conditions. The second step is characterized by reaching the equilibrium due to the saturation of the surface and pores structure with IC molecules. The adsorption curves of contact time indicate possible monolayer coverage of IC on the nanocomposites surface. In addition, it has been mentioned that GO could be photocatalytically degraded the IC more easily than the AgNPs/GO nanocomposites [38]. The incorporation of AgNPs was proposed to inhibit the adsorption of IC and the degradation was reduced. The oxidation properties of GO and r-GO have also been reported elsewhere [54]. Therefore, it can be noted that the presence of Mn_2O_3 in both of PANI/ Mn_2O_3 and GO/PANI/ Mn_2O_3 led to decreases their adsorption capacity comparing with PANI and GO/PANI, respectively. It is well known that metal oxides are comparatively heavy and possess lower surface area to weight ratio as compared to PANI or GO, so an excessive increase in the amount of metal oxide in the composites, results in a reduction of the adsorption capacity [55], the determined specific surface area of the different composites confirmed the above aspect as shown in Table 3. Moreover, the MnO_3 surface can be coverage with adsorbed SO_4^{2-} anions, thus, working as a dopant for PANI chains. Although, this negative influence of the presence of MnO_2 on adsorption capacity for IC, but their uses as a solid oxidant for the synthesis of this ternary

Table 3 The specific surface areas determined by IC adsorption (S_{IC}), for the four PANI composites

| Composite | $S_{IC} \times 10^{-3} \text{ km}^2/\text{kg}$ |
|--|--|
| GO/PANI ($S_2O_8^{2-}$ as an oxidant) | 149.56 |
| GO/PANI/ Mn_2O_3 | 142.14 |
| PANI ($S_2O_8^{2-}$ as an oxidant) | 131.01 |
| PANI/ MnO_2 | 48.84 |

nanocomposite may be an advantage from the environmental point of view.

Effect of Initial Dye Concentration

The effect of initial IC concentration on the adsorption efficiency of the adsorbents under investigation was studied and evaluated using various concentrations of IC and the results are shown in Fig. 7. It is clear that increasing the initial IC concentration led to decrease the removal percentage of IC at a constant amount of GO/PANI (5 mg). This result revealed that sorption efficiency and adsorption capacity showed opposite trends against an increase in initial IC concentration Fig. 8. When the dye concentration was increased from 36.50 to 54.73 mg/L, the percentage removal of IC decreased from 87.5 to 64.06%. In general, there are many parameters that could influence the adsorption of dyes such as; surface charge, the chemical composition of the dye, adsorbent surface properties, hydrophobic and hydrophilic nature, hydrogen bonding, electrostatic interaction, steric effect, a van der Waals forces, and so forth [56]. As expected, when the concentration of IC was increased, the limited capacity of the adsorption checks any

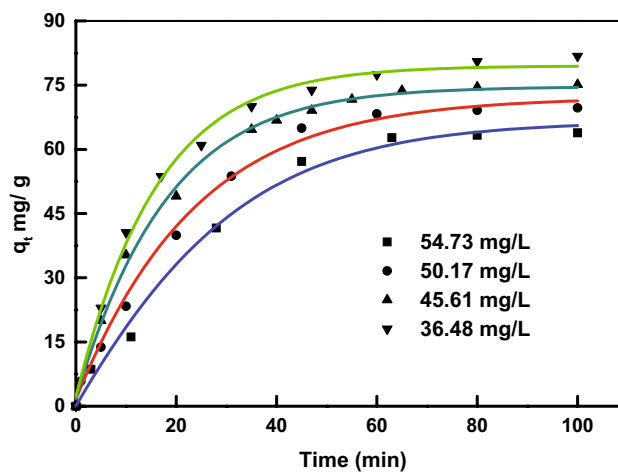


Fig. 7 Effect of initial concentration on the adsorption of IC onto GO/PANI/ Mn_2O_3 composite (5 mg/L) at 30 °C

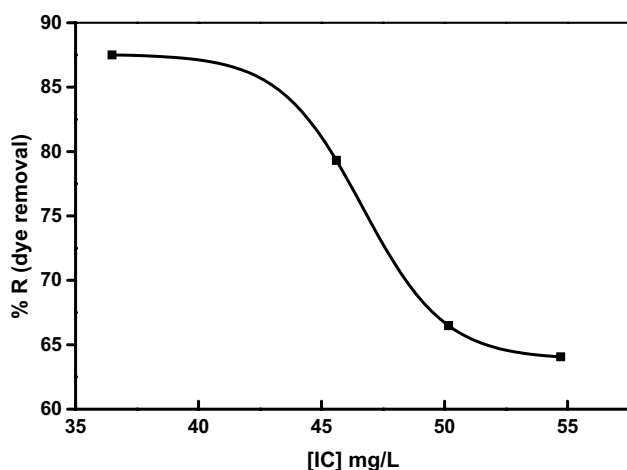


Fig. 8 Dependence of adsorption efficiency on initial dye concentration (adsorbent dose = 5 mg, $t = 30^\circ\text{C}$)

further adsorption of dye and hence the overall removal percentage decreases.

Effect of Adsorbent Dosage

The adsorbent dose is an important parameter in the determination of adsorption capacity. The effect of the adsorbent dose was investigated by the addition of various amounts of GO/PANI adsorbent from 5 to 12 mg in 10 mL aqueous solutions of IC (45.61 mg/L) at room temperature for equilibrium time. It was observed that the removal efficiency of IC increased from 79.31 to 90.42% with increasing adsorbent dosage. This can be attributed to the greater surface area and availability of more adsorption sites.

Effect of pH

The effect of solution pH is one of the most important factors for adsorption efficiency since there are various charging characteristics of ionic-type adsorbents under different pH conditions resulting in variant affinity to contaminants. Generally, adsorption process is dependent on the zero point of charge (zpc) of adsorbent as well as the pK_a value of the dye. i.e. more specifically on the electrostatic interaction between the adsorbent and the pollutant. The pK_a value of IC has determined from the pH dependence of electronic absorption spectra of dilute IC solution was equal to 12.3. The effect of pH on the reaction rate was studied at constant concentrations of the dye as well as fixed amount of the GO/PANI composite at 30°C . The pH was changed in the (5.5–11) range using the phosphate buffer of 0.067 M and few drops of NaOH were added to obtain the higher pH values. The results indicated that change of the initial pH (pH_0) of the dye solution has a negligible effect on the

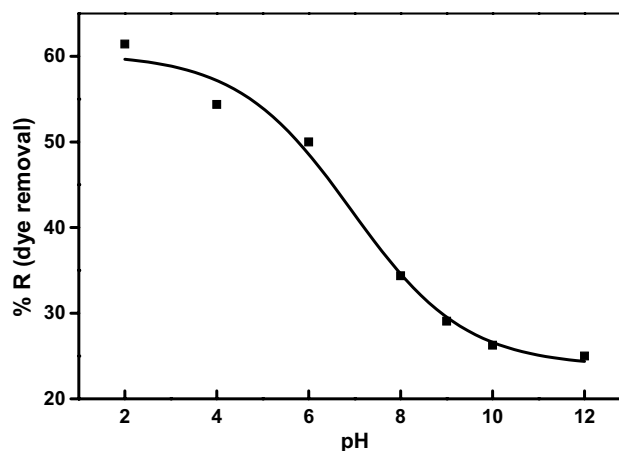


Fig. 9 Dependence of adsorption efficiency of IC ($C_0 = 45.61$ mg/L, on pH, adsorbent dose = 5 mg, $t = 30^\circ\text{C}$)

λ_{max} of IC. This observation provides evidence that at this range of pH, there is no any change in the chemical structural of the dye molecules. Figure 9 demonstrates the relation between the pH and the removal percentage of IC. It is clear the adsorption of IC was highest at lower pH, while it shows a sharp decreasing in the strong alkaline medium. The pH_{ZPC} of GO/PANI composite was determined and equals 9.5. This means that at $\text{pH} < \text{pH}_{\text{ZPC}}$, the adsorbent surfaces were net positively charged, while at $\text{pH} > \text{zpc}$ the surface of the adsorbent were negatively charged. Thus, the observed dependence of IC removal on the solution pH can be attributed to the variation of the adsorbent surface charges. At lower pH, the surface of GO/PANI or GO/PANI/ Mn_2O_3 is positively charged due to the dissociation and released of the dopant SO_4^{2-} ions, with simultaneous protonation of imines nitrogen atoms of PANI matrix and the adsorption of H^+ ions on the Mn_2O_3 surface. Therefore, the anionic IC molecules could be attracted via electrostatic force by the positively charged active sites of the surface of the composite. To ensure the release of SO_4^{2-} ions, the adsorption batch filtrate was treated with BaCl_2 solution, which gives a white precipitate of BaSO_4 . On the other hand, the decrease of removal capacity at higher pH values could be attributed to the deprotonation of imines nitrogen atoms, carboxylate groups of GO and the competitive interactions between OH^- ions of buffer solution and the anionic IC molecules present on adsorption solution. Moreover, at $\text{pH} > 12$, IC may be exhibited intra-molecular hydrogen bonding network between the carbon, oxygen atoms, and N–H within the molecule [56]. These hydrogen bonds cause a weakness of the N–H bond in the IC molecule results in the strong intermolecular interactions (e.g. H-bonding) of the N–H group to NH groups of the PANI chains.

Table 4 Comparison of adsorption capacity of various adsorbents towards the removal of IC

| Adsorbent | q _m (mg/g) | Refs. |
|--|-----------------------|-----------|
| Rice husk ash | 29.27 | [58] |
| Carbonaceous materials | 92.83 | [59] |
| Sewage sludge | 60.04 | [55] |
| PVA/SiO ₂ nanofiber membranes | 40.60 | [62] |
| Pyrolyzed sewage sludge | 30.82 | [60] |
| GO/PANI | 88.73 | This work |
| GO/PANI/Mn ₂ O ₃ | 76.40 | This work |

Table 5 Thermodynamic parameters for the adsorption of IC onto GO/PANI

| Temp. (K) | ΔG° (kJ/mol) | ΔH° (kJ/mol) | ΔS° (kJ/mol K) |
|-----------|--------------|--------------|----------------|
| 303 | -38.22 | | |
| 305 | -36.98 | | |
| 308 | -35.74 | -113.49 | -0.248 |
| 313 | -34.49 | | |

Thermodynamic Study of Adsorption

The thermodynamic parameters provide in-depth information about the internal energetic change that is associated with adsorption process. Thus, the adsorption of IC was studied at different temperatures of 30, 35, 40, and 45 °C (Table 4), and under the optimal conditions of initial IC concentration of 1 × 10⁻⁴ M. The equilibrium adsorption capacity of GO/PANI increased from 34.20 to 76.67 mg/g with decreasing the temperature from 45 to 30 °C, indicating that the adsorption of IC is an exothermic process. Both of ΔH° and ΔS° values were determined from the linear plot of ln (q_e/C_e) and 1/T according to Eyring Eq. (5). In addition, the value of ΔG° was determined from Eq. (6).

$$(q_e/C_e) = \Delta S^\circ/R - \Delta H^\circ/RT \tag{5}$$

$$\Delta G^\circ = \Delta H^\circ - T \Delta S^\circ \tag{6}$$

where R is the universal gas constant 8.314 J/(mol K), T is the absolute temperature (K), q_e equilibrium adsorption capacities, and C_e is the equilibrium concentration (mol/L). The negative standard free energy change (ΔG°) indicated that the adsorption was the spontaneous process and the value of ΔG° became more negative with the decrease of temperature, indicating that lower temperature facilitated the adsorption of IC on GO/PANI composite, Table 5. The negative ΔH° value suggested an exothermic and the chemisorption nature of the adsorption of IC. The negative standard entropy change (ΔS°) reflected decreased randomness at the solid–liquid interface during the adsorption of IC on GO/PANI composites. For comparison, the maximum adsorption capacities of IC using other adsorbents are presented in Table 4, [55–61]. Thus, it is clear that our composites have a high adsorption capacity for IC removal relative to the other carbon-based adsorbents.

Adsorption Kinetics

Kinetic models were used to study the controlling mechanism of the adsorption process. The time-dependent adsorption of IC onto GO/PANI was studied at different initial concentrations, based on the linear concentrations range of IC. Three models were applied to test experimental data and thus elucidate the kinetic of the adsorption process. The highest regression coefficient R² values were considered as the fitness of the model for the adsorption process. The linearized form of the pseudo-first-order, Eq. (7), is expressed as follows:

$$\log (q_e - q_t) = \log (q_e) - k_1/2.303 t \tag{7}$$

where k₁ is the first-order rate constant of adsorption. k₁ and q_e were determined from the slope and intercept of the plot of log (q_e–q_t) against t. The values of k₁ and the Pearson correlation coefficient are summarized in Table 6. It has been found that the experimental q_e values, did not agree with the calculated values obtained from the linear plots. It suggests that the kinetics of IC adsorption did not follow the pseudo-first-order kinetic model. Thus, pseudo-second order kinetic model given by Equ.(8) [62] was applied;

Table 6 Parameters of pseudo-first order, pseudo-second order, and intraparticle diffusion models for the adsorption of IC

| [IC] ₀ mg/L | Pseudo first order model | | | Pseudo-second order model | | | | Intraparticle diffusion model | | | |
|------------------------|--------------------------------------|-------------------------------------|----------------|---------------------------|---------------------------|--|----------------|--|----------------|---|----------------|
| | q _e (mg g ⁻¹) | k ₁ (min ⁻¹) | R ² | q _{e,cal} (mg/g) | q _{e,exp} (mg/g) | k ₂ × 10 ⁻³ (g/mg min) | R ² | K _{p1} /10 ⁻³ (mol g ⁻² min ^{-1/2}) | R ² | K _{p1} /10 ⁻³ mol/g ⁻¹ min ^{-1/2} | R ² |
| 36.48 | 81.60 | 0.0618 | 0.988 | 64.35 | 63.84 | 0.836 | 0.994 | 7.670 | 0.0964 | 5.96 | 0.931 |
| 45.61 | 80.58 | 0.0622 | 0.994 | 70.00 | 69.67 | 0.920 | 0.996 | 8.800 | 0.984 | 6.54 | 0.927 |
| 50.17 | 80.75 | 0.0598 | 0.996 | 76.11 | 75.12 | 1.050 | 0.998 | 11.14 | 0.996 | 3.04 | 0.983 |
| 54.73 | 73.62 | 0.0500 | 0.997 | 81.56 | 81.73 | 1.090 | 0.999 | 13.06 | 0.997 | 4.74 | 0.962 |

$$(t/q_t) = (1/k_2 q_e^2) + (t/q_e) \quad (8)$$

where k_2 is the rate constant of pseudo-second-order (g/mol/min). The parameters k_2 , q_e , and R^2 values were determined and are listed in Table 6. It is clear that the R^2 values were significantly better fitted for the pseudo-second-order kinetic than a pseudo-first-order kinetic model for all IC concentrations, indicating the applicability of this kinetic model to describe the adsorption process, which suggested that the adsorption process is controlled by chemisorption. Moreover, the experimental data were also used for intraparticle diffusion model, Eq. (9):

$$q_t = k_p t^{0.5} + C \quad (9)$$

where k_p is the intraparticle diffusion rate constant (mol/g min^{0.5}) and C is a constant (mol/g) that gives information about the thickness of the boundary layer. The larger of the C value, the greater is the boundary layer effect [63]. The intraparticle diffusion constant, k_p , and the correlation coefficient, R^2 were calculated and listed in Table 6. The values of k_p give an idea about the thickness of boundary layer. Generally, it is well known that the adsorption takes place through two stages, a bulk diffusion step followed by intraparticle diffusion [64]. In the first stage, the dye is transported from solution through the particle/solution interface and characterized by kp^1 . In the second stage, the IC molecules diffuse onto the interlayers of GO/PANI composites and consequently get adsorbed by the interior surface of each sheet which is measured by kp^2 . At this stage, the diffusion resistance increases and causes a decrease in the diffusion rate. The values of kp^1 and kp^2 calculated from the slopes of the two intersecting segments are given in Table 6, where $kp^1 > kp^2$. With the continuous uptake of the IC from the solution, the adsorption was decreased with lower diffusion rate until the final equilibrium was reached.

Adsorption Isotherms

Adsorption isotherm indicates how adsorbate molecules distribute between the liquid phase and solid phase at equilibrium. Several equations have been employed for analyzing the experimental adsorption equilibrium data. The Langmuir model assumes that the adsorption occurs on a homogenous surface by monolayer coverage with no subsequent interaction between adsorbed species. The linear form of the Langmuir model is represented by Eq. (10);

$$C_e/q_e = (1/K_L q_{max}) + (C_e/q_{max}) \quad (10)$$

where C_e is the equilibrium concentration of the adsorbate (mg/L), q_e is the amount of adsorbate adsorbed per unit mass of adsorbent (mg/L), K_L is the Langmuir adsorption

constant (L/mg), and q_{max} is the theoretical maximum adsorption capacity (mg/g). The values of K_L and q_{max} were determined and are listed in Table 6. The essential characteristic of Langmuir equation can also be expressed in terms of a dimensionless separation factor R_L given in Eq. (11);

$$R_L = 1/(1 + K_L C_o) \quad (11)$$

where K_L is the Langmuir isotherm constant (L/mg), and C_o is the initial IC concentration (mg/L). The R_L value indicates the type of the isotherm to be either favorable ($0 < R_L < 1$), unfavorable ($R_L > 1$), linear ($R_L = 1$) or irreversible ($R_L = 0$) [59]. The value of R_L in the present investigation was found to be 0.90 at 30 °C indicating that the adsorption of IC on GO/PANI is favorable.

The Freundlich isotherm described the adsorption where the adsorbent has a heterogeneous surface with adsorption sites that have different energies of adsorption. The energy of adsorption varies as a function of the surface coverage (q_e) and is represented by the Freundlich constant K_F (L/g) [56] as specified in Eq. (12);

$$\ln q_e = \ln K_F + (1/n) \ln C_e \quad (12)$$

where K_F and n are the Freundlich constants related to the adsorption capacity and adsorption intensity, respectively, q_e is the equilibrium amount of adsorbed IC per gram of GO/PANI composite and C_e is the equilibrium concentration of IC in solution. The magnitude of n varies with the heterogeneity of the adsorbent and for the favorable adsorption process, the value of it should be less than 10 and higher than unity [64]. The values of K_F and $1/n$ together with the correlation coefficient, R^2 are listed in Table 7.

Temkin considered the effects of some indirect adsorbent/adsorbate interactions on adsorption isotherms and suggested that the heat of adsorption of all the molecules in the layer would decrease linearly with surface coverage [59]. The Temkin isotherm has been applied in the following form:

$$q_e = B_1 \ln K_t + B_1 \ln C_e \quad (13)$$

where $B = RT/b$, b is the Temkin constant related to the heat of sorption (J/mol); K_t is the Temkin isotherm constant (L/g), R is the gas constant (8.314 J/mol K) and T is the absolute temperature (K). As seen in Table 7, the Langmuir isotherm fits quite well with the experimental data (correlation coefficient $R^2 > 0.99$), whereas, the low correlation coefficients ($R^2 = 0.94, 0.92$) show the poor agreement of Freundlich and Temkin isotherms of the experimental data. The fact that the Langmuir isotherm fits the experimental data very well may be due to the homogeneous distribution of active sites onto GO/PANI composites surface.

Table 7 Parameters of Langmuir, Freundlich, and Temkin isotherm models and correlation coefficients for IC adsorption

| Model | Condition for applicability | Parameters | Values of the parameters | |
|------------|---|-----------------------|--------------------------|--|
| | | | GO/PANI | GO/PANI/Mn ₂ O ₃ |
| Langmuir | Monolayer adsorption or homogeneous surface | q _m (mg/g) | 88.73 | 76.40 |
| | | K _L (L/mg) | 0.487 | 0.438 |
| | | R ² | 0.992 | 0.997 |
| Freundlich | Multi-layers adsorption or non-uniform distribution | K _F (L/g) | 50.76 | 40.48 |
| | | n | 6.366 | 5.418 |
| | | R ² | 0.954 | 0.949 |
| Temkin | Uniform distribution or heterogeneous surface | B _T | 75.27 | 169.90 |
| | | K _T (L/g) | 1.866 | 1.222 |
| | | R ² | 0.922 | 0.935 |

Conclusions

The idea to incorporate multi-solid components into a composite form in the one-pot method is attractive to evaluate their synergetic effect on the adsorption of organic dyes. Graphene oxide/polyaniline composites using MnO₂ as an oxidant have been synthesized and used as an effective adsorbent for the removal of IC from aqueous solution. The possible combining mode of GO/PANI/Mn₂O₃ composite is proposed including (a) π - π stacking (b) electrostatic interactions, and (c) hydrogen bonding, while the presence of Mn₂O₃ particles and their surface adsorbed ions could be functioned as dopant ions for PANI chains. The Langmuir isotherm model was found to more suitable to describe adsorption, suggesting monolayer coverage of IC molecules on the adsorbent surface. The adsorption capacity of GO/PANI increased from 34.20 to 76.67 mg/g with decreasing the temperature from 45 to 30 °C, indicating that the adsorption of IC is an exothermic process. The dye adsorption followed the pseudo-second-order kinetics. Evaluation of thermodynamic parameters revealed that the adsorption process is exothermic and spontaneous. The role of each component of the composite was evaluated. It can be concluded the present method is promising and can be considered as one of those methods devoted to treating the wastewater streams with low cost.

Acknowledgements This work is supported and funded by Tanta University, Faculty of Science, Chemistry Department.

Compliance with Ethical Standards

Conflict of interest The authors declare that they have no conflicts of interest.

References

- Novoselov KS, Geim AK, Morozov SV et al (2004) Electric field effect in atomically thin carbon films. *Science* 306:666–669
- Schedin F, Geim A, Morozov S et al (2007) Detection of individual gas molecules adsorbed on graphene. *Nat Mater* 6:652–655
- Li D, Müller MB, Gilje S et al (2008) Processable aqueous dispersions of graphene nanosheets. *Nat Nanotechnol* 3:101–105
- Park S, Ruoff RS (2009) Chemical methods for the production of graphenes. *Nat Nanotechnol* 4:45–47
- Mauter MS, Elimelech M (2008) Environmental applications of carbon-based nanomaterials. *Environ Sci Technol* 42:5843–5859
- Liu Z, Duan X, Zhou X et al (2014) Controlling and formation mechanism of oxygen-containing groups on graphite oxide. *Ind Eng Chem Res* 53:253–258
- Gao W (2015) The chemistry of graphene oxide. In: Gao W (ed) *Graphene oxide: Reduction recipes, spectroscopy, and applications*, chap 3. Springer, New York, pp 61–95
- Song J, Wang X, Chang C-T et al (2014) Preparation and characterization of graphene oxide. *J Nanomater* 2014:1–6
- Martínez-Orozco RD, Rosu HC, Lee SW, Rodríguez-González V (2013) Understanding the adsorptive and photoactivity properties of Ag-graphene oxide nanocomposites. *J Hazard Mater* 263:52–60
- Iturbe-Ek J, Andrade-Martínez J, Gómez R, Rodríguez-González V (2015) A functional assembly of SiO₂ nanospheres/graphene oxide composites. *Mater Lett* 142:75–79
- Pyun J (2011) Graphene oxide as catalyst: application of carbon materials beyond nanotechnology. *Angew Chem Int Edit* 50:46–48
- Huang J (2006) Syntheses and applications of conducting polymer polyaniline nanofibers. *Pure Appl Chem* 78:15–27
- Bhadra S, Khastgir D, Singha NK, Lee JH (2009) Progress in preparation, processing and applications of polyaniline. *Prog Polym Sci* 34:783–810
- Sen T, Mishra S, Shimpi NG (2016) Synthesis and sensing applications of polyaniline nanocomposites: a review. *RSC Adv* 6:42196–42222
- Wang H, Hao Q, Yang X et al (2010) Effect of graphene oxide on the properties of its composite with polyaniline. *ACS Appl Mater Interfaces* 2:821–828

16. Kim M, Lee C, Seo YD et al (2015) Fabrication of various conducting polymers using graphene oxide as a chemical oxidant. *Chem Mater* 27:6238–6248
17. Kumar NA (2012) Polyaniline-grafted reduced graphene oxide for efficient electrochemical. *ACS Nano* 25:1715–1723
18. Xu LQ, Liu YL, Neoh KG et al (2011) Reduction of graphene oxide by aniline with its concomitant oxidative polymerization. *Macromol Rapid Commun* 32:684–688
19. Gemeay AH, El-Sharkawy RG, Mansour IA, Zaki AB (2007) Preparation and characterization of polyaniline/manganese dioxide composites and their catalytic activity. *J Colloid Interface Sci* 308:385–394
20. Bhaiswar JB, Dongre MYSSP, Kinge R et al (2015) Application of PANI/MnO₂ nanocomposite in ultrasonics. *Inter J Sci Res* 22–24. 419–421
21. Jaidev, Jafri RI, Mishra AK, Ramaprabhu S (2011) Polyaniline–MnO₂ nanotube hybrid nanocomposite as supercapacitor electrode material in acidic electrolyte. *J Mater Chem* 21:17601
22. Gemeay AH, El-Sharkawy RG, Mansour IA, Zaki AB (2008) Catalytic activity of polyaniline/MnO₂ composites towards the oxidative decolorization of organic dyes. *Appl Catal B Environ* 80:106–115
23. Bhaumik M, McCrindle R, Maity A (2013) Efficient removal of congo red from aqueous solutions by adsorption onto interconnected polypyrrole-polyaniline nanofibres. *Chem Eng J* 228:506–515
24. Wang J, Deng B, Chen H (2009) Removal of aqueous Hg (II) by polyaniline: sorption characteristics and mechanisms. *Environ Sci Technol* 43:5223–5228
25. Mahanta D, Madras G, Radhakrishnan S, Patil S (2008) Adsorption of sulfonated dyes by polyaniline emeraldine salt and its kinetics. *J Phys Chem B* 112:10153–10157
26. Li K, Guo D, Chen J et al (2015) Oil-water interfacial synthesis of graphene-polyaniline-MnO₂-hybrids using binary oxidant for high-performance supercapacitor. *Synth Met* 209:555–560
27. Li K, Guo D, Lin F et al (2015) Electrosorption of copper ions by poly(m-phenylenediamine)/reduced graphene oxide synthesized via a one-step in situ redox strategy. *Electrochim Acta* 166:47–53
28. Saggiore EM, Oliveira AS, Buss DF et al (2015) Photo-decolorization and ecotoxicological effects of solar compound parabolic collector pilot plant and artificial light photocatalysis of indigo carmine dye. *Dye Pigment* 113:571–580
29. Barka N, Assabbane A, Nounah A, Ichou YA (2008) Photocatalytic degradation of indigo carmine in aqueous solution by TiO₂-coated non-woven fibres. *J Hazard Mater* 152:1054–1059
30. Jeffords DL, Lance PH, Dewolf WC (1977) Severe indigo. *Urology* IX:180–181
31. Mededovic S, Takashima K (2008) Decolorization of indigo carmine dye by spark discharge in water. *Int J Plasma Environ Sci Technol* 2:56–64
32. Dogdu G, Yalcuk A (2015) Indigo dyeing wastewater treatment by eco-friendly constructed wetlands using different bedding media. *Desalin Water Treat.* 57(32):1–13
33. Hammami S, Oturan M a., Oturan N et al (2012) Comparative mineralization of textile dye indigo by photo-fenton process and anodic oxidation using boron-doped diamond anode. *Desalin Water Treat* 45:297–304
34. Lorimer JP, Mason TJ, Plattes M, Phull SS (2000) Dye effluent decolourisation using ultrasonically assisted. *Ultrason Sonochem* 7:237–242
35. Galindo C, Jacques P, Kalt A (2001) Photochemical and photocatalytic degradation of an indigoid dye: a case study of acid blue 74 (AB74). *J Photochem Photobiol A Chem* 141:47–56
36. Xu LQ, Yang WJ, Neoh KG et al (2010) Dopamine-induced reduction and functionalization of graphene oxide nanosheets. *Macromolecules* 43:8336–8339
37. Rao CNR, Sood AK, Subrahmanyam KS, Govindaraj A (2009) Graphene: the new two-dimensional nanomaterial. *Angew Chem Int Edit* 48:7752–7777
38. Martinez-Orozco RD, Rosu HC, Lee SW, Rodroguéz-Gonzalez V (2013) Understanding the adsorptive and photoactivity properties of Ag-graphene oxide nanocomposites. *J Hazard Mater* 263:52–60
39. Kovtyukhova NI, Ollivier PJ, Martin BR et al (1999) Layer-by-layer assembly of ultrathin composite films from micron-sized graphite oxide sheets and polycations. *Chem Mater* 11:771–778
40. Han G, Liu Y, Zhang L et al (2014) MnO₂ nanorods intercalating graphene oxide/polyaniline ternary composites for robust high-performance supercapacitors. *Sci Rep* 4:4824
41. Huang YF, Lin CW (2012) Polyaniline-intercalated graphene oxide sheet and its transition to a nanotube through a self-curling process. *Polymer* 53:1079–1085
42. Wang G, Tang Q, Bao H et al (2013) Synthesis of hierarchical sulfonated graphene/MnO₂/polyaniline ternary composite and its improved electrochemical performance. *J Power Sour* 241:231–238
43. Gemeay AH, Mansour IA, El-Sharkawy RG, Zaki AB (2005) Preparation and characterization of polyaniline/manganese dioxide composites via oxidative polymerization: effect of acids. *Eur Polym J* 41:2575–2583
44. Nguyen VH, Tang L, Shim JJ (2013) Electrochemical property of graphene oxide/polyaniline composite prepared by in situ interfacial polymerization. *Colloid Polym Sci* 291:2237–2243
45. Li Y, Xiang Y, Dong X et al (2009) Polymerization of aniline in the interlayer space of molybdenum trioxide and its electrochemical properties. *J Solid State Chem* 182:2041–2045
46. Posudievsky OY, Biskulova SA., Pokhodenko VD (2002) New polyaniline–MoO₃ nanocomposite as a result of direct polymer intercalation. *J Mater Chem* 12:1446–1449
47. Chen F, Liu P, Zhao Q (2012) Well-defined graphene/polyaniline flake composites for high-performance supercapacitors. *Electrochim Acta* 76:62–68
48. Liu Y, Deng R, Wang Z, Liu H (2012) Carboxyl-functionalized graphene oxide–polyaniline composite as a promising supercapacitor material. *J Mater Chem* 22:13619
49. Xu MW, Zhao DD, Bao SJ, Li HL (2007) Mesoporous amorphous MnO₂ as electrode material for supercapacitor. *J Solid State Electrochem* 11:1101–1107
50. Chen CH (2003) Thermal and morphological studies of chemically prepared emeraldine-base-form polyaniline powder. *J Appl Polym Sci* 89:2142–2148
51. Fan X, Peng W, Li Y et al (2008) Deoxygenation of exfoliated graphite oxide under alkaline conditions: a green route to graphene preparation. *Adv Mater* 20:4490–4493
52. Zhang L, Jamal R, Zhao Q et al (2015) Preparation of PEDOT/GO, PEDOT/MnO₂, and PEDOT/GO/MnO₂ nanocomposites and their application in catalytic degradation of methylene blue. *Nanoscale Res Lett* 10:148
53. Lee M, Yang S, Kim K et al (2014) Comparison of the catalytic oxidation reaction on graphene oxide and reduced graphene oxide. *J Phys Chem C* 118:1142–1147
54. Li M, Wang H, Wu S et al (2012) Adsorption of hazardous dyes indigo carmine and acid red on nanofiber membranes. *RSC Adv* 2:900–907
55. Otero M, Rozada F, Calvo LF et al (2003) Elimination of organic water pollutants using adsorbents obtained from sewage sludge. *Dye Pigment* 57:55–65
56. Lakshmi UR, Srivastava VC, Mall ID, Lataye DH (2009) Rice husk ash as an effective adsorbent: evaluation of adsorptive

- characteristics for Indigo Carmine dye. *J Environ Manag* 90:710–720
57. Gutiérrez-Segura E, Solache-Ríos M, Colín-Cruz A (2009) Sorption of indigo carmine by a Fe-zeolitic tuff and carbonaceous material from pyrolyzed sewage sludge. *J Hazard Mater* 170:1227–1235
 58. Dalaran M, Emik S, Guclu G et al (2011) Study on a novel poly-ampholyte nanocomposite superabsorbent hydrogels: synthesis, characterization, and investigation of removal of indigo carmine from aqueous solution. *Desalination* 279:170–182
 59. Jiwalak N, Rattanaphani S, Bremner JB, Rattanaphani V (2010) Equilibrium and kinetic modeling of the adsorption of indigo carmine onto silk. *Fibers Polym* 11:572–579
 60. Jia Y, Jin Q, Li Y et al (2015) Investigation of the adsorption behavior of different types of dyes on MIL-100(Fe) and their removal from natural water. *Anal Methods* 7:1463–1470
 61. Prasad AL, Santhi T (2012) Adsorption of hazardous cationic dyes from aqueous solution onto *Acacia nilotica* leaves as an eco-friendly adsorbent. *Sustain Environ Res* 22:113–122
 62. Ghaedi M, Sadeghian B, Pebdani AA et al (2012) Kinetics, thermodynamics and equilibrium evaluation of direct yellow 12 removals by adsorption onto silver nanoparticles loaded activated carbon. *Chem Eng J* 187:133–141
 63. Arami M, Limaee NY, Mahmoodi NM, Tabrizi NS (2006) Equilibrium and kinetics studies for the adsorption of direct and acid dyes from aqueous solution by soy meal hull. *J Hazard Mater* 135:171–179
 64. Chang J, Ma J, Ma Q et al (2016) Adsorption of methylene blue onto Fe₃O₄/activated montmorillonite nanocomposite. *Appl Clay Sci* 119:132–140